Proceedings of the 3rd International Conference on Fluid Flow and Thermal Science (ICFFTS'22)
~~Seoul, South Korea~~ Virtual Conference - October 27 - 29, 2022
Paper No. 113
DOI: 10.11159/icffts22.113

Control of Flow Separation Based on Karman Vortex Generator for a Planar Diffuser

Sikai Li[1] and Huanxin Lai[1]
[1]School of Mechanical and Power Engineering, East China University of Science and Technology,
130 Meilong Road, Xuhui District, Shanghai, P. R. China
15726987868@163.com; hlai@ecust.edu.cn

Abstract - Diffusers are the elements for converting the kinetic energy of fluid into pressure, by changing the area of cross section. A large expansion angle is usually adopted for diffusers in application for compaction of the devices. However, when the expansion angle is increased, a wide range of flow separation will occur due to the negative pressure gradient. Such separation will eventually lead to a failure in the performance of the diffuser. For controlling of flow separation, positive and/or negative strategies are often employed.In this paper, the method of using the Karman Vortex Generator (KVG) to control flow separation is explored. Different from applying the KVG in upstream of the separation point, the KVG is applied at the throat of the diffuser in this paper. Large Eddy Simulations (LES) is employed to calculate the flow in a planar diffuser at Re=9000. The expansion angle θ=25°, and area ratio AR=2. With the combined effects of viscous force and adverse pressure gradient, flow separation occurs at the throat of the diffuser. KVG is applied at several positions in nearby of the separation point. The calculation results show that at the separation point, a properly set KVG can make the spanwise vortices fully interact with the low-energy fluid near the wall surface, and as a result, the separation bubble is well suppressed.

***Keywords*:** Karman-Vortex Generator, separation control, LES, planar diffuser

1. Introduction

Diffusers are important part of turbomachinery, which realize the mutual conversion between dynamic pressure and static pressure through the change of flow area[1]. The adverse pressure gradient in the two-dimensional diffuser depends on its divergence angle (θ) and constant area ratio (AR). Performance of diffusers is usually evaluated by the conversion efficiency relative to the length of the expansion section. So, in practical engineering, diffuser with larger expansion angle is usually preferred when ensuring the area ratio. However, with the increase of the expansion angle, the intensified geometric expansion of the throat usually leads to the appearance of large-scale separation bubbles there, causing the decrease of the effective flow area and pressure recovery efficiency[2]. In order to obtain a compact diffuser structure and high performance at the same time, certain flow control methods are often employed in practical engineering.

The flow control method is divided into active methods and passive methods. Although active control methods have significant effects, they usually require additional equipment to achieve energy injection. By contrast, the passive control method is more economical, simpler in structure, and easier to implement in engineering. At present, many mature passive control devices have been developed, such as traditional vane vortex generators, backward wedge and forward wedge vortex generators, etc. [3-6] They achieve their control effect by the excitation of the stream-wise vortex after the device to the near-wall low energy fluid. Veldhuis[7] compared the control effect of these conventional vortex generators and out-of-surface cylinder which is a new type of vortex generator, found that out-of-surface cylinder has great potential in suppressing flow separation. The periodic spanwise vortex generated by the cylinder is different from the stream-wise vortex after the traditional vortex generator, that can achieve the periodic incentive to the near-wall area. Zhang[8] referred to the above cylindrical vortex generators as Karman Vortex Generators (KVG). Cylindrical structures similar to KVG are also widely used to achieve other functions such as suppressing flow separation after square columns and cylinders, enhancing heat transfer, etc., most of them are set upstream of the separation region. Although the control effect of KVG has gradually gained attention, the research on KVG is not as extensive as that of traditional VG, and its control mechanism and setting principles are not completely clear. At the same time, it should be pointed out that for the flow control of the diffuser, most of the previous work choose to place the KVG at a certain distance upstream of the separation region to generate vortex street for flow control, but they rarely pay attention to the control effect of the KVG near the separation point which is equally effective.

For this reason, this paper selects the plane diffuser calculated by Yang[9] as the baseline diffuser, designs several groups of KVGs with different sizes and locations near the separation point, and employs the large eddy simulation (LES) method to compare the flow control efficiency of different set KVGs. On the basis of comprehensive analysis of the flow physics of the diffuser and flow characteristics around the circular cylinder, the flow control mechanism and design principles of KVG are discussed.

2. Numerical settings and calculation settings

2.1. Flow Control Models

The geometric dimensions and flow parameters of the baseline diffuser in this paper refer to the calculation example of Yang[9]. The diffuser expansion angle and area ratio are θ =25° and AR= 2, respectively. The inlet channel height, the upstream channel length and spanwise width of the throat are 2δ, 100δ and 2δ, respectively. The expansion section of the diffuser starts from x/δ=0 to x/δ=5.4, and smoothly connects the inlet and outlet by a fillet with a radius of 5δ. The streamwise computational domain extends to x/δ=30.

A KVG is arranged near the separation point to suppress the flow separation, as shown in Figure 1(a). The KVG is illustrated by a green solid circle, D_k denotes the diameter of KVG, L_t and G represent the horizonal distance and the vertical distance from the wall, respectively. The size and position of the KVG are determined by these three parameters. Regarding the settings of D_k and G, Zhang[8] and Yang[9] considered that D_k and G/D_k=2-3, which account for 3%-4% of the length of the expansion segment, are reasonable choices. In addition, considering the size of the diffuser, the flow characteristics and the development of the wake of KVG, L_t/D_k=0-4 is set, which basically covers the location of the separation point, and is arranged at the front end of the throat, which can be directly affected by the incoming flow. A structured grid is adopted for the entire computational domain. Grid settings refer to the fine grid setting of Ref. [10], with a total of 3.66 million cells. The grid in expansion section and the near-wall area are refined, and the grid near the KVG is divided by an O-shaped grid, as shown in Figure 2(b).

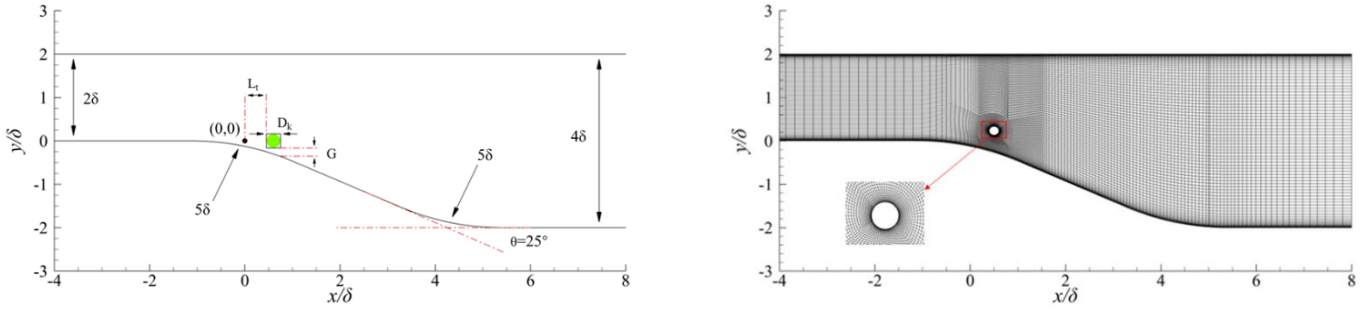

Fig 1: (a) Sketch of the KVG setting; (b) front view of the grid settings of a controlled diffuser.

2.2 Numerical Methods and Boundary condition

Set the boundary condition of the inlet as the velocity inlet, the average inflow Mach number M_a=0.2, Reynolds number $Re=\rho U_m\delta/\mu$=9000, where ρ represent the density, U_m is the average inflow velocity, δ and μ denote the half-height of the upstream channel and dynamic viscosity, respectively, the reference static pressure is 101325Pa; the spanwise direction is set as the periodic boundary condition; the normal boundary is defined as the non-slip wall; the outlet is set as the outflow boundary.

The initial flow in this paper is established by the steady SST k-ω turbulence model. The Density-Based solver is utilized for the calculation, and the bounded central difference scheme and the second-order implicit scheme are employed for spatial discretization and time advance, respectively. In order to accurately predict the flow separation under the adverse pressure gradient, the Dynamic Smagorinsky model, which has good performance in predicting this type of flow referring to the study of Ref. [10], is selected as the subgrid model. Setting the time step of LES as 0.14δ/Um, corresponding to the full-field *CFL*

(Courant-Friedrichs-Lewy) ≤1. After the calculation of 600δ/U_m, unsteady flow has been fully developed, and the influence of the initial field is basically disappeared, the statistical analysis of the data is carried out on this basis.

3. Results and Discussion

3.1 Numerical validation

For the convenience of expression, this paper makes the following explanation of the symbols: u，v，w和u'，v'，w' represent the instantaneous and corresponding fluctuation velocities in the x, y, z directions respectively; "$\bar{}$" and "$\langle\ \rangle$" are the time and spanwise averaged operators, For example, $\langle\bar{u}\rangle$ represents averaged velocity both in time and spanwise direction; the static pressure recovery coefficient C_{spr} and total pressure recovery coefficient C_{tpr} at the end of the expansion section which quantifies the performance of diffuser are defined by equations (1) and (2), respectively, where p_s and p_t represent static pressure and total pressure, respectively , the subscripts "1" and "2" represent the inlet channel position x=-5δ and the end of expansion section x=5.4δ; the ideal static pressure coefficient C_{ispr} of the diffuser is obtained by equation (3).

$$C_{spr}=\frac{1/A_2\int\overline{p_{s2}}dA_2-1/A_1\int\overline{p_{s1}}dA_1}{0.5\rho U_m^2}=\frac{\left(P_{S2}-P_{S1}\right)}{0.5\rho U_m^2} \tag{1}$$

$$C_{tpr}=\frac{1/A_2\int\overline{p_{t2}}dA_2}{1/A_1\int\overline{p_{t1}}dA_1}=P_{t2}/P_{t1} \tag{2}$$

$$C_{ispr}=1-1/AR^2 \tag{3}$$

Figure 2 shows the velocity distribution in the expansion section of this paper. It can be seen that the result of this paper is in good agreement with the calculation results of Yang [9], and there is only a slight difference at the peak. The size of the separation bubble and the pressure recovery performance of the diffuser are shown in Table 1. The predicted position of the separation point and the height of the separation bubble are basically consistent with the simulation of Yang [9]. As for the prediction of reattachment point and static pressure recovery coefficient, the calculation results of this paper are lower than the referencing results, but the errors are maintained at around 3%, and the overall results coincide well which indicating that the calculation method of this paper is feasible in the simulation of diffusion separation flow.

According to equation (3), the ideal static pressure recovery coefficient of the diffuser in this paper is 0.75, while the static pressure recovery coefficient calculated is only 0.2328. In fact, the static pressure continues to increase in the downstream of the end of expansion section, reaching a maximum value at x/δ=25. When replace the p_{s2} in Eq. (1) with the area-weighted average static pressure at x/δ = 25.0, C_{spr} is 0.5467 which coincide well with Yang's calculation results, and is considered reasonable according to the research in Ref [2].

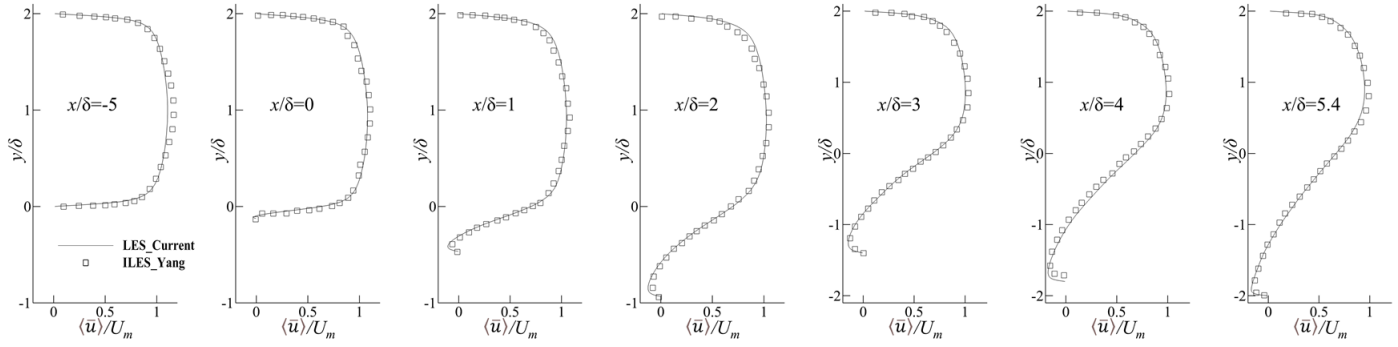

Fig 2: Time and spanwise averaged streamwise velocity at some locations.

Table 1: size of separation bubble and static pressure recovery performance of diffuser

Data source	Method	Separation point	Reattachment point	Bubble length	Bubble height	C_{spr}
Yang	ILES	-0.31δ	10.38δ	10.69δ	0.77δ	0.2412
This paper	LES	-0.33δ	10.12δ	10.45δ	0.76δ	0.2328

3.2 Mean Flow Analysis

The large eddy simulation based on the dynamic Smagorinsky model is employed to calculate controlled cases, the performance of different KVGs is shown in Table 2. The results show that the flow control effect largely depends on the position and size of the KVG. Different KVG settings can not only effectively improve the performance of the diffuser, but also deteriorate its pressure conversion efficiency. All the controlled cases have a small variation in Ctpr, which is caused by the low inflow velocity, the dynamic pressure accounts for only 2.3% of the total pressure. The comparison of the control efficiency of different KVGs shows that Dk=0.15-0.2δ, which are equivalent to 3%-4% of the length of the expansion section, and G/Dk=2-3 are very reasonable parameter ranges near the separation point. Lt/Dk=0 performs poorly compared to other locations. The scheme of Case 10 achieves the best performance in improving pressure recovery performance, compared to uncontrolled case, the Cspr and Ctpr are increased by 55% and 0.06%, respectively. Case 3 and Case 7 perform worst and moderate among all the controlled cases, respectively. In order to study the control mechanism of KVG, the above three cases with the uncontrolled diffuser are compared.

Table 2: Comparisons of the different Karman-vortex generatorss

Case	D_k	L_t/D_k	G/D_k	C_{spr}	C_{tpr}
1	0.15	0	2	0.2576	0.9916
2	0.15	0	3	0.1417	0.9899
3	0.15	2	2	0.2990	0.9924
4	0.15	2	3	0.3029	0.9925
5	0.15	4	2	0.2550	0.9916
6	0.2	0	2	0.2421	0.9914
7	0.2	0	3	0.0785	0.9888
8	0.2	2	2	0.3035	0.9923
9	0.2	2	3	0.3089	0.9921
10	0.2	4	2	0.3623	0.9927
uncontrolled	-	-	-	0.2328	0.9921

Figures 3 show the streamlines and flow velocity distributions in the throat. It can be seen that for the uncontrolled configuration, under the combined effect of the adverse pressure gradient and geometric expansion, the flow separation starts near the starting point of the expansion point and evolves into a large recirculation area, and the high-speed flow is confined in a small range, which eventually leads to a decrease in the performance of the diffuser. Compared with the uncontrolled case, although there are local backflows and regions behind the cylinder that the velocity changes drastically due to the KVG wake and blockage in the controlled configuration. Under the effective control of KVG, separation bubble in the throat is Significantly reduced, the flow area is increased. However, the KVG in Case 7 did not play an effective control role, because the KVG was so far from the wall surface that the wake fails to stimulate the low-energy fluid near the wall surface.

The time and spanwise averaged turbulent kinetic energy (TKE) is defined by $k = 0.5\left\langle \overline{u'u'} + \overline{v'v'} + \overline{w'w'} \right\rangle$ .The normalized turbulent kinetic energy distribution is shown in Fig. 4. All cases captured maximum TKE in near-wall region upstream, which corresponds to fully developed channel. For the uncontrolled case, strong velocity fluctuation is caused by the instability of the shear layer generated by flow separation at the throat, and maintains a high level until the end of the expansion section. Under the periodic excitation of the KVG wake vortex, the development of the separation bubble is interrupted, severe turbulence level only existed in a short distance behind the cylinder, and the TKE level in the second half of the throat is significantly reduced. A proper set KVG near the separation point effectively improves the flow quality downstream.

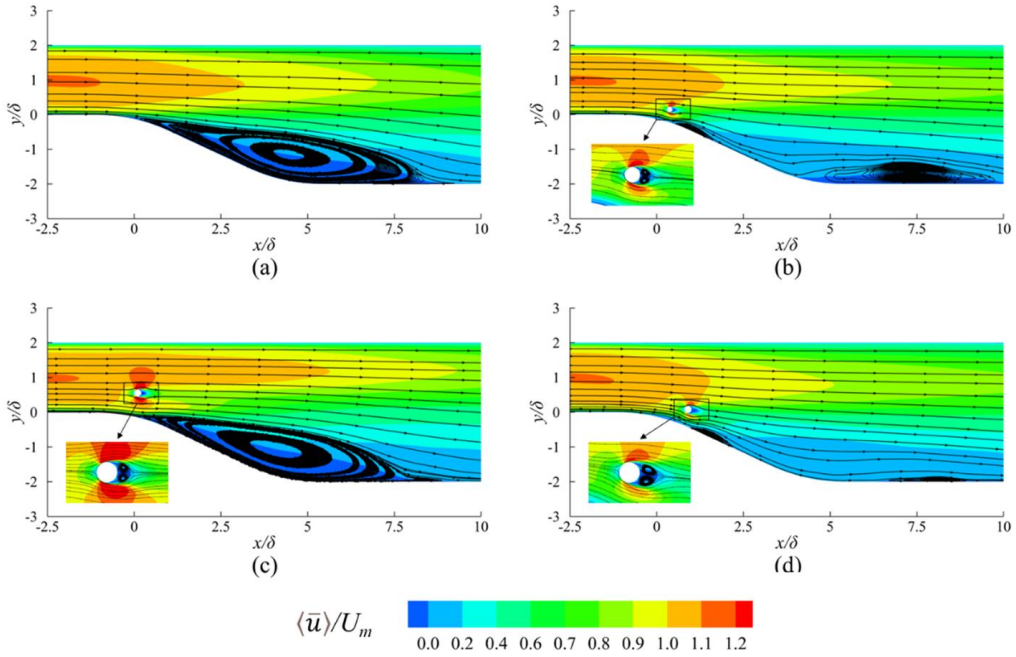

Fig 3: Streamlines of the time and spanwise averaged velocity. (a)Uncontrolled case; (b)Case 3; (c)Case 7; (d)Case10.

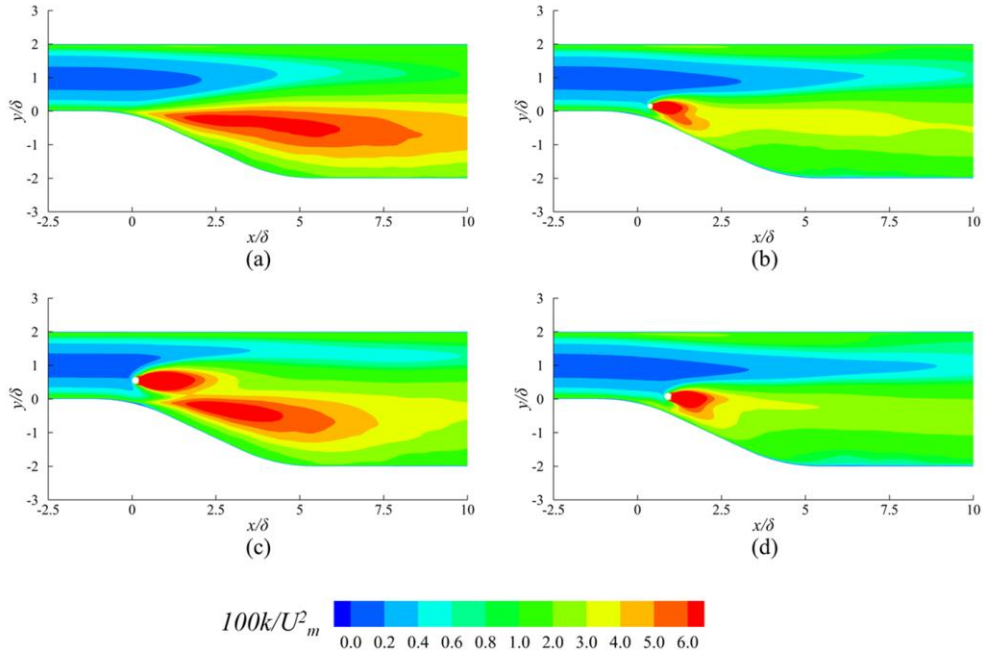

Fig 4: Time and spanwise averaged turbulent kinetic energy distribution. (a)Uncontrolled case; (b)Case 3; (c)Case 7; (d)Case10.

The time and spanwise average static pressure recovery coefficient is defined by $C_p = \left(\left\langle \overline{p_S} \right\rangle - P_{S1}\right) / 0.5\rho U^2{}_m$, which characterizes the pressure change in the expansion section. Figure 5 shows the time and spanwise average static pressure distributions of the four operating conditions. Since the development of the separation bubble is not blocked in the uncontrolled configuration, the development of the flow is limited in a small range and the high-speed flow is maintained to a greater extent, as a result the conversion efficiency of kinetic energy to pressure is reduced. In the controlled case, a local high-pressure area appears at the front end of all KVGs which is due to the blocking effect of the KVG on the incoming flow. The accelerated fluid on both sides of the KVG and the wake vortex cause a blue low-pressure area to appear on the sides and behind of the cylinder, but this area lasts short in space, and the pressure recovers quickly in the latter half of the throat. Finally at the effective control of the KVG, the development of separation bubbles is inhibited, the effective flow area is increased, and the pressure recovery coefficient at the end of the expansion section is improved.

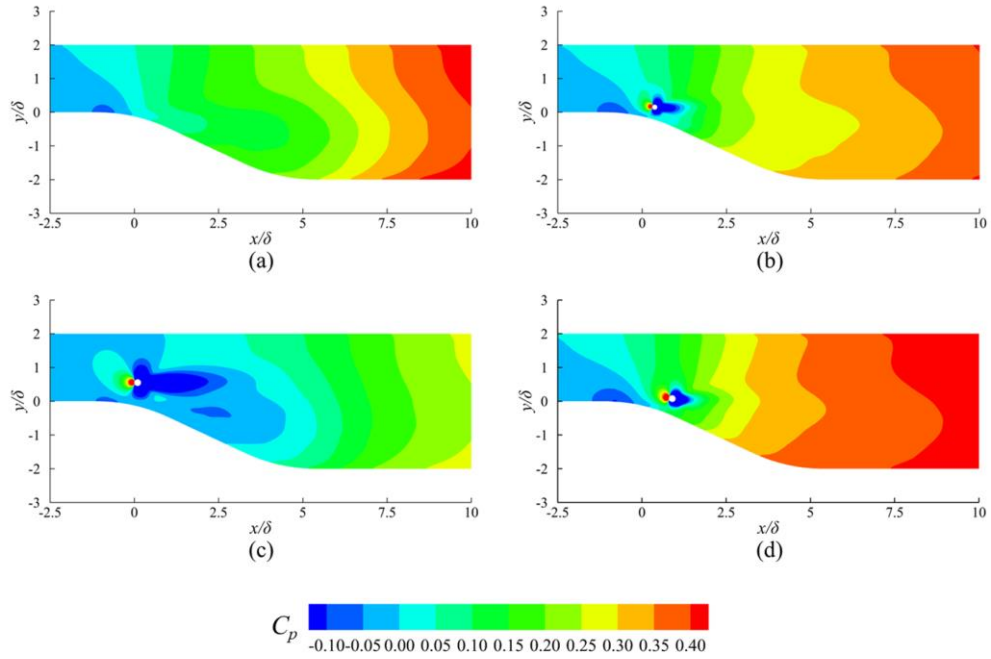

Fig 5: Time and spanwise averaged static pressure distribution. (a)Uncontrolled case; (b)Case 3; (c)Case 7; (d)Case10.

3.3 Instantaneous Flow Field and Frequency Characteristics

The flow separation of the expanding section is closely related to the transient vortex structure. Figures 6 and Figure 7 show the instantaneous spanwise vorticity distribution in the throat. Under the combined effect of geometric expansion and adverse pressure gradient, the rapid velocity change leads to the appearance of velocity shear layer. Due to the instability of the shear layer, vortices in different scales are generated, which continue to evolve, roll up, break up and merge, resulting in a highly unsteady flow in the throat.

In the controlled configuration, the shedding of Karman vortex pairs is captured in all operating conditions. It can be observed in the Case 3 and Case 10 that the KVG wake vortex interacts with the near-wall vortex, resulting in the development of the Karman vortex street being blocked and broken up to small-scale vortices, indicating that KVG enhances the flow mixing in the near-wall region by additionally introducing a periodic Karman vortex street, thereby achieving the effect of inhibiting the flow separation of the expansion section.

The frequency characteristics of the flow field based on pressure are shown in Fig. 8. Two sampling points located at the wake of the KVG and end of the expansion section, respectively. From the Fourier analysis, in the uncontrolled diffuser, the flow in the expansion section is highly unsteady due to the strong turbulent effect of the separation bubbles. No obvious frequency peaks are observed at either point. For the effectively controlled Case 10 diffuser, the peak frequency predicted by LES in point 1 is about St = 0.79. When normalize the St = 0.79 by the KVG diameter $D_k = 0.2\delta$ and local velocity $U_k = 0.77U_m$, the Reynold number Re_k=1386 and Strouhal number St_k=0.205, respectively, which corresponds to the Karman vortex shedding frequency at current Reynolds number. The secondary frequency St=1.57 is close to twice the primary frequency, which is caused by the drag characteristic of KVG due to the second harmonic frequency. In addition, the power spectral density of Case 10 at point 1 is slightly higher than that of the uncontrolled diffuser at $St > 0.7$, because the small-scale vortices are more abundant in the throat under control, as shown in Fig. 7. As the flow reaches the end of the expansion section, the low-frequency part of the control configuration at point 2 is lower than uncontrolled diffuser, the magnitude of the power spectral density of the high-frequency part is basically the same, and the signal of the Karman-vortex shedding are already hard to observe, which suggesting that the unsteadiness caused by KVG may decay rapidly.

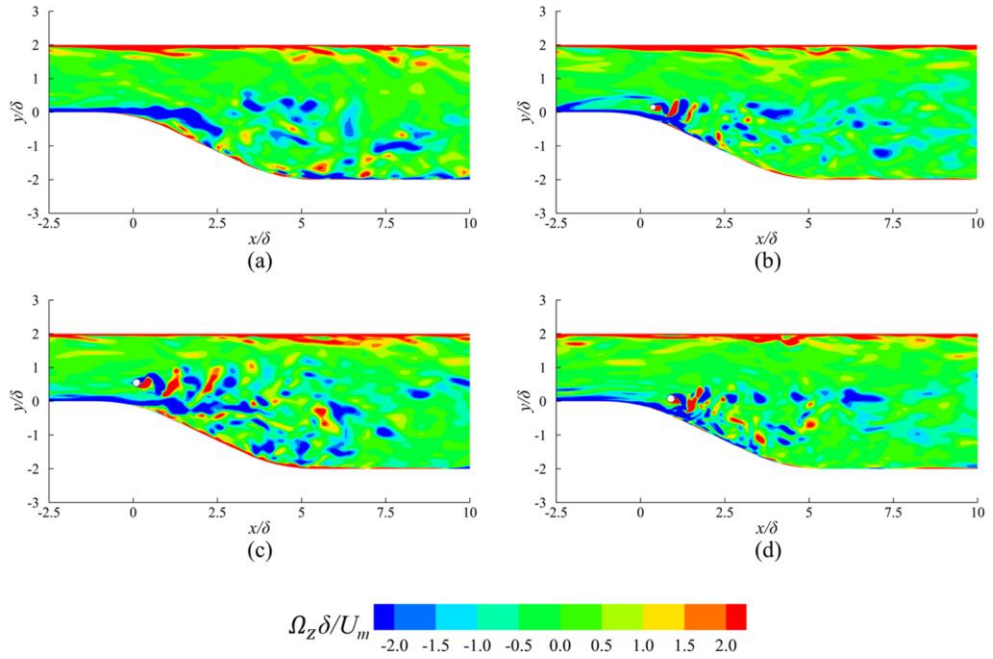

Fig 6: Instantaneous Ω_z distributions at slice $z/\delta = 2.0$ for different cases. (a)Uncontrolled case; (b)Case 3; (c)Case 7; (d)Case10.

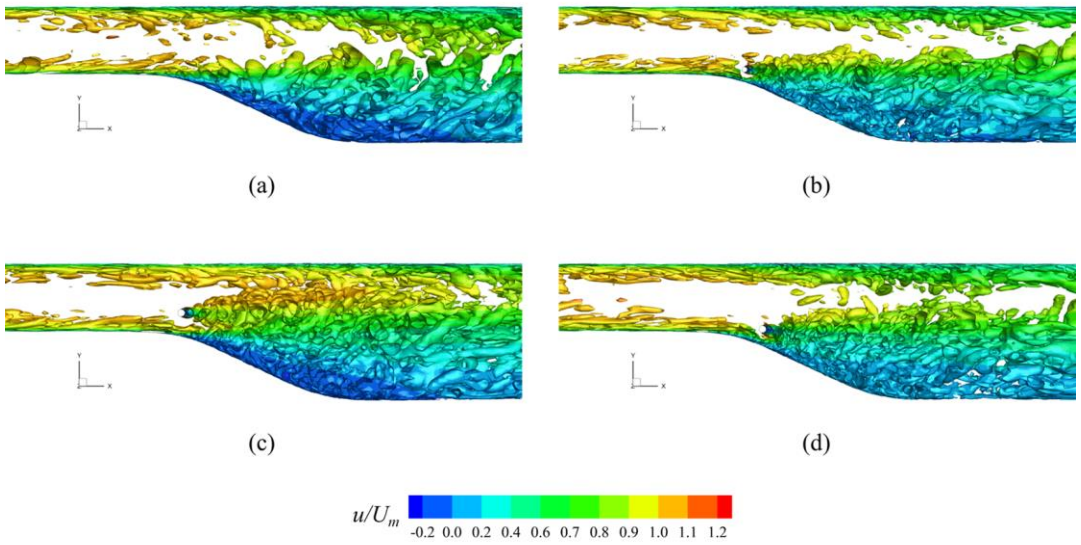

Fig7: Vortical structure distributions characterized by the iso-surface of $Q(\delta/U_m)^2 = 0.1$, colored by instantaneous streamwise velocity. (a)Uncontrolled case; (b)Case 3; (c)Case 7; (d)Case10.

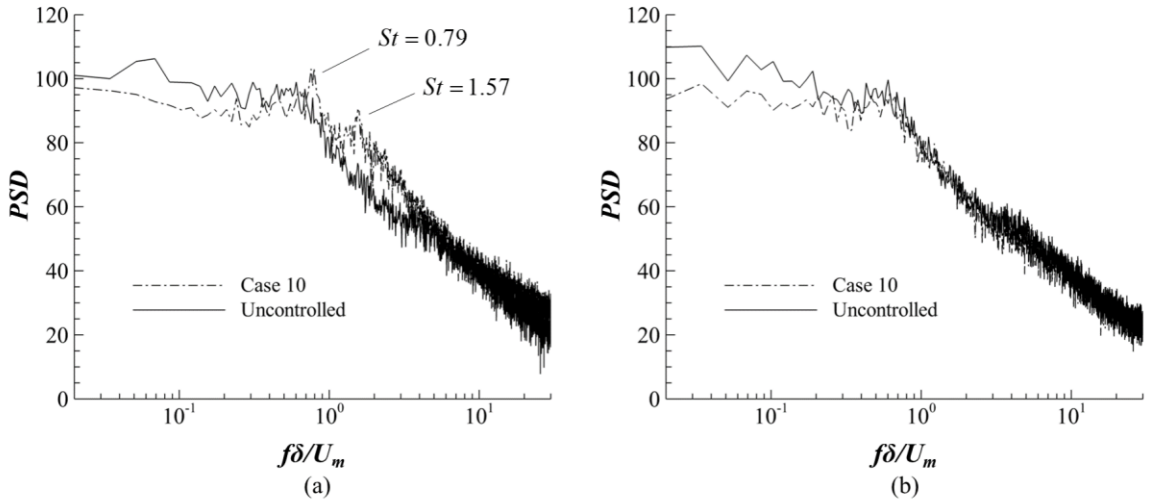

Fig 8: Pressure frequencies at two sample points of the flow field. (a) point (2δ,0) (b) point (5.4δ,0).

4. Conclusion

In this paper, large eddy simulation is employed to study the flow control effect of KVG in the plane diffuser. The results show that reasonably arranged KVG near the separation point can make the spanwise vortex fully interact with the low-energy fluid near the wall, effectively suppress the generation of separation bubbles, and improve the performance of the diffuser. The KVG control effect is sensitive to its position and size. The KVG diameter D_k equivalent to 3%-4% of the length of the expansion section and the vertical distance G/D_k=2-3 are very reasonable choices near the separation point, and the horizontal distance L_t/D_k=2-4 is a suitable range. D_k=0.2δ, L_t/D_k=4, G/D_k=2 are the best combinations obtained in this paper.

Acknowledgement

This study is funded by the NSFC under Grant 51976061.

References

[1] L. R. Reneau, J. P. Johnston, and S. J. Kline, “Performance and design of straight, two-dimensional diffusers,” J. Basic Eng.89(1), 141 (1967).
[2] G. N. Patterson, “Modern diffuser design: The efficient transformation of kinetic energy to pressure,” Aircr. Eng. Aerosp. Technol.10(9), 267–273 (1938).
[3] A. C. Brown, H. F. Nawrocki, and P. N. Paley, “Subsonic diffusers designed integrally with vortex generators,” J. Aircr.5(3), 221–229 (1968).
[4] G. Tanguy, D. G. MacManus, P. Zachos, “Passive flow control study in an S-duct using stereo particle image velocimetry,” AIAA J.55(6), 1862–1877 (2017)
[5] J. C. Lin, “Review of research on low-profile vortex generators to control boundary-layer separation,” Prog. Aeros. Sci.38(4-5), 389–420 (2002)
[6] M. Sajben, C. P. Chen, and J. C. Kroutil, “A new passive boundary-layer control device,” J. Aircr.14(7), 654–660 (1977).
[7] L. Veldhuis and M. van der Steen, “Flow separation control by off surface elements,” in 28th AIAA Applied Aerodynamics Conference (AIAA, 2010), p. 4684.
[8] Y. F. Zhang, H. X. Chen, and S. Fu, “A Karman-vortex generator for passive separation control in a conical diffuser,” Sci. China Phys., Mech. Astron.55(5), 828–836 (2012).
[9] Yang J, Zhang Y, Chen H, Unsteady flow control of a plane diffuser based on a Karman-vortex generator[J]. AIP

Advances, 2020, 10(5):055314.
[10] Tang H, Lei Y, Li X, Large-Eddy Simulation of an Asymmetric Plane Diffuser: Comparison of Different Subgrid Scale Models[J]. Symmetry, 2019, 11(11):1337.